



1 **Multisatellite observations of the magnetosphere response to changes in the solar wind and**
2 **interplanetary magnetic field**

3

4 Galina Korotova^{1,2}, David Sibeck³, Scott Thaller⁴, John Wygant⁴, Harlan Spence⁵, Craig
5 Kletzing⁶, Vassilis Angelopoulos⁷, and Robert Redmon⁸

6

7 ¹IPST, University of Maryland, College Park, MD, USA

8 ²IZMIRAN, Russian Academy of Sciences, Moscow, Troitsk, Russia

9 ³Code 674, NASA/GSFC, Greenbelt, MD, USA

10 ⁴College of Science and Engineering, University of Minnesota, Minneapolis, MN, USA

11 ⁵EOS, University of New Hampshire, Durham, NH, USA

12 ⁶Department of Physics and Astronomy, Iowa University, Iowa City, IA, USA

13 ⁷Department of Earth, Planetary and Space sciences, UCLA, Los Angeles, CA, USA

14 ⁸Solar and Terrestrial Physics division, NGDC/NOAA, Boulder, CO, USA

15

16 **Abstract**

17 We employ multipoint observations of the magnetosphere to present case and statistical
18 studies of the electromagnetic field and plasma response to interplanetary (IP) shocks. On
19 February 27, 2014 the initial encounter of an IP shock with the magnetopause occurred on the
20 early postnoon magnetosphere, consistent with the observed alignment of the shock with the
21 spiral IMF. The dayside equatorial magnetosphere exhibited a dusk-dawn oscillatory electrical
22 field with a period of ~ 330 s and peak to peak amplitudes of ~ 15 mV/m for a period of 30
23 min. The intensity of electrons in the energy range from 31.5 to 342 KeV responded with
24 periods corresponding to the shock induced ULF electric field waves. The initial electric field
25 perturbation was directed downward for this case study. We then perform a statistical study of
26 Ey variations of the electric field and associated plasma drift V_x and V_y flow velocities for 30
27 magnetospheric events during the passage of interplanetary shocks. The direction of the initial
28 V_x component of plasma flow is tailward at all local times except the nightside magnetosphere,
29 where flows are sunward near the sun-Earth line but antisunward towards dawn and dusk. The
30 observed directions of the azimuthal velocity V_y predominately agree with those expected for
31 the given spiral or orthospiral shock normal orientation.

32 **Introduction**



33 Sudden increases in the solar wind dynamic pressure accompanying interplanetary (IP)
34 shocks cause earthward motion of the bow shock and the magnetopause and launch fast and
35 intermediate mode waves into the magnetosphere [Tamao, 1964]. The fast mode waves
36 propagate both radially inward and azimuthally around the Earth [Araki et al., 1997] whereas the
37 intermediate mode waves propagate along magnetic field lines to produce transient perturbations
38 in the high-latitude dayside ionosphere [Southwood and Kivelson, 1990; Glaßmeier and
39 Heppner, 1992]. Using multipoint observations Wilken et al. [1982] estimated the propagation
40 speeds to be about 600 km/s in the radial direction from geostationary orbit to the ground and
41 about 910 km/s in the azimuthal direction in the equatorial plane. Nopper et al. [1982] estimated
42 an impulse disturbance speed of about 1500 km/s at geostationary orbit. Schmidt and Pedersen
43 [1988] derived a propagation velocity for the radially inward travelling compressive wave of 950
44 km/s and for the azimuthal wave in the outer magnetosphere of 1100 km/s. Samsonov et al.
45 [2007] used a magnetohydrodynamic code to simulate the interaction of a moderately strong
46 interplanetary shock propagating along the Sun-Earth line and obtained the average speed of the
47 primary and reflected fast shocks in the magnetosphere to be about 700 km/s, in agreement with
48 their assumptions concerning the mean Alfvén velocity in the outer dayside magnetosphere
49 (1000 km/s) and in the plasmasphere (500 km/s).

50 The IP shock orientation plays an important role in determining the associated geophysical
51 effects [e.g., Oliveira and Raeder, 2015]. Guo et al. [2005] showed that system evolution times
52 are much longer for shocks with normals oblique to the Sun–Earth line. The pressure pulse
53 model of Sibeck et al. [1990] predicts dawnward moving transient events near local noon when
54 shock normals point perpendicular to the nominal spiral interplanetary magnetic field (IMF)
55 direction, but duskward moving events occur near local noon for events when shock normals
56 point perpendicular to the orthospiral IMF orientation. The direction of the plasma flow
57 within the magnetosphere is expected to be consistent with the orientation of the shock. That
58 is to say dawnward flow for spiral IMF shocks and duskward flow for orthospiral IMF shocks.
59 Here orthospiral refers to IMF longitudes ($0^\circ < \Lambda < 90^\circ$ and $180^\circ < \Lambda < 270^\circ$), spiral refers to IMF
60 longitudes ($90^\circ < \Lambda < 180^\circ$ and $270^\circ < \Lambda < 360^\circ$), where longitude $\Lambda=0^\circ$ points sunward, and
61 $\Lambda=90^\circ$ duskward.



62 The magnetic and electric fields are key parameters for understanding of the response of
63 the Earth's space environment to IP shocks. The propagation and evolution of electric fields in
64 the magnetosphere-ionosphere system in response to IP shocks have been studied for several
65 decades but signatures of the shock related electric field perturbations are still not fully
66 understood. Knott et al. [1985] reported that the electric field observed by the GEOS-2 satellite
67 showed a transient signature of about 7 mV/m in the dayside magnetosphere associated with the
68 onset of a Sudden Commencement (SC). These signatures were followed by Pc4-5 oscillations.
69 Schmidt and Pedersen [1988] performed a statistical investigation of the GEOS2 electric field
70 signatures associated with SC that showed a clear tailward flow pattern near local noon. Close to
71 the flanks or in the nightside of the magnetosphere the corresponding flows also exhibited a
72 radially inward component. Shinbory et al [2004] investigated the detailed signatures of the
73 Akebono electric and magnetic fields associated with SCs inside the plasmasphere ($L < 5$). The
74 initial excursion of the electric field associated with SCs was almost directed westward at all
75 local times. The amplitude did not show a clear dependence on magnetic local time and the
76 intensity of the E_y field gradually increased by 0.5-2.0 mV/m about 1-2 minutes after the onset
77 of the initial electric field impulse. The propagation velocity of SCs disturbances derived from
78 the amplitude ratio of the electric field to magnetic field was about 360 km/s in the equatorial
79 plasmasphere. Kim et al. [2009] used an MHD simulation to examine the electric field and
80 suggested that the SC associated electric field seen by Shinbory et al. [2004] was the convection
81 electric field. Takahashi et al. [2017] investigated the spatial and temporal evolution of large-
82 scale electric fields in the magnetosphere and ionosphere associated with SCs using multipoint
83 equatorial magnetospheric and ionospheric satellites together with ground radars and showed
84 that the propagation characteristics of electric fields in the equatorial plane depend on magnetic
85 local time. They showed that the initial variation of the electric field (negative E_y) lasted about
86 one minute and was directed westward throughout the inner magnetosphere. Positive E_y
87 became dominant 2 min after SCs propagated to pre-midnight or post-midnight region with
88 near constant amplitude.

89 Observations and MHD simulations [e.g., Li et al., 1993; Zong et al., 2009; Halford et al.,
90 2014; Schiller et al., 2016] show that the electric fields generated by sudden compressions can
91 resonantly interact with trapped charged particle populations within the Earth magnetosphere,



92 energizing and injecting them deep into the magnetosphere. During the well-known shock
93 event in March 1991, the CRESS satellite observed injected electrons energized to extremely
94 high energies, up to 5 MeV [Blake et al., 1992]. Wygant et al. [1994] showed that the shock
95 related electric and magnetic field perturbations observed by the CRRES satellite in the
96 nightside inner magnetosphere exhibited a bipolar waveform with amplitude of about 80 mV/m
97 and 140 nT, respectively, and energized the energetic electrons to energies up to 15 MeV. Foster
98 et al. [2015] found that a shock with an azimuthal electric field impulse of 10 mV/m observed
99 by the Van Allen Probes was responsible for accelerating 1.5-4.5 MeV electrons by 400 KeV
100 in the radial region of $L= 3.5-4$.

101 This paper focuses on two major issues. We will inspect multispacecraft electric and
102 magnetic field and particles and plasma observations to study their response to an IP shock on
103 February 27, 2014. We will time the occurrence of magnetic field disturbances associated with
104 the shock in space and the magnetosphere and will determine the direction of their propagation.
105 Then we will perform a statistical study of the Van Allen Probes electric field disturbances in the
106 magnetosphere and associated plasma drift V_x and V_y velocities in response to IP shocks. We
107 will investigate how the electric field perturbations deviate from the preceding undisturbed
108 period during shock-induced compressions and whether the signatures of the shock electric
109 field perturbations have a clear dependence on magnetic local time. We will study whether the
110 direction of the shock normal has any effect on the propagation of the shock induced magnetic
111 and plasma disturbances. We will compare our statistical results to the results of MHD
112 simulations.

113

114 **Data sets**

115 The extensive Van Allen Probes, THEMIS, Cluster and GOES multi-instrument data sets
116 provide numerous opportunities to observe the magnetospheric response to the changes in the
117 solar wind and interplanetary magnetic field monitored by Wind. The five THEMIS spacecraft
118 were launched in 2007 and carry identical instruments and operated in highly elliptical, near-
119 equatorial, orbits that precess about the Earth with apogees of 12, 20, and 30 RE and orbital
120 periods of 1, 2, and 4 days. With the outermost two spacecraft ARTEMIS now at the Moon,
121 three THEMIS spacecraft remain on the innermost orbits. We use magnetic field data with 3 s



122 time resolution data from the THEMIS FGM triaxial fluxgate magnetometers [Auster et al.,
123 2008]. The ESA electrostatic analyzer on the THEMIS spacecraft measures the distribution
124 functions of 0.005 to 25 keV ions and 0.005 to 30 keV electrons over 4 π -str and provides
125 accurate 3 s time resolution plasma moments, pitch angle and gyrophase particle distributions
126 [McFadden et al., 2008].

127 The two Van Allen Probes were launched in August 2012 into nearly identical equatorial
128 and low inclination ($\sim 10^\circ$) orbits with perigee altitudes of 605 and 625 km and apogee altitudes
129 of 30410 and 30540 km [Mauk et al., 2012]. Both satellites carry identical sets of instruments to
130 measure charged particle populations, fields, and waves in the inner magnetosphere. In this
131 paper, we employ observations from the Energetic Particle, Composition, and Thermal Plasma
132 Suite (ECT: MagEIS, 20-4000 keV for electrons) [Spence et al., 2013; Blake et al., 2013].
133 Electric and Magnetic Field Instrument Suite and Integrated Science (EMFISIS) [Kletzing et al.,
134 2013], and the Electric Field and Waves Suite (EFW) [Wygant et al., 2013]. In particular, we
135 inspect electric and magnetic field observations with 11 and 4 s time resolution, respectively,
136 and differential particle flux measurements with ~ 11 s (spin period) time resolution. The electric
137 field data were obtained from sites <http://www.space.umn.edu/rbspew-data> and CDAWEB where
138 they are presented in an MGSE (modified GSE) coordinate system. They provide two
139 components Y and Z of the electric field. Both components are in the spin plane of the spacecraft
140 and are measured with the 50 m long booms. The spin axis X is oriented within 37 degrees of
141 the Earth-Sun line. The spin axis component of the electric field can be obtained from the $\mathbf{E} \cdot$
142 $\mathbf{B} = 0$ assumption. For this to succeed the magnetic field should be at least 15 degrees out of the
143 spin plane. To calculate Van Allen Probes plasma flow velocities we converted the electric field
144 data from modified MGSE coordinates into GSE coordinates. Additionally we used magnetic
145 field data from GOES 13 and 15 with 0.5 s time resolution [Singer et al., 1966] and Cluster with
146 4 s time resolution [Balogh et al., 1997]. We use Wind solar wind magnetic field and SWE
147 plasma data with 3 s [Lepping et al., 1995] and 1 min, respectively [Ogilvie et al., 1995].

148 **Observations**

149 Figure 1 presents Wind magnetic and plasma data from 15:30 to 16:10 UT on February 27,
150 2014. The arrival of the shock at Wind at 15:50 UT (X, Y, Z GSM = (220.9, 93.9, 30.7 Re)) is
151 revealed by an enhancement in the interplanetary magnetic field strength from 6 to 16 nT and



152 total plasma velocity from 350 to 420 km/s. The IMF had positive B_x and negative B_y
153 components during the whole interval that both increased the shock arrived. The solar wind
154 density increased from 18 to 45 cm^{-3} , and the dynamic pressure increased from 3 to 13 nPa. This
155 fast forward (FF) shock was oblique. Its normal was calculated using magnetic field coplanarity
156 and pointed in the GSM coordinates directions of $[n_x, n_y, n_z] = [0.72, 0.39, 0.56]$, i.e., it was
157 aligned with the spiral shock orientation. We will use the direction of the shock normal to
158 interpret the timing results for the IP shock arrival observed by THEMIS, GOES, Cluster and the
159 Van Allen Probes spacecraft for this event.

160 Figure 2 shows the GSM locations of The THEMIS, Cluster, Van Allen Probes and GOES
161 spacecraft at $\sim 16:50$ UT (Their coordinates are given in Table 1). All the spacecraft located in
162 the solar wind observed the enhanced the magnetic field strength, densities, velocities and
163 temperatures associated with the IP shock. The shock induced disturbances were seen just
164 upstream from the bow shock by Cluster 2 and 1 at 16:48:44 UT and 16:48:46 UT, respectively .

165 Figures 3 (a, b) show the THEMIS D and A observations of the magnetic field, plasma and
166 energy spectra of ion fluxes from 16:40 to 17:20 UT. The spacecraft were initially located in the
167 magnetosheath. At 16:49:01 UT the IP shock hit THEMIS D as indicated by enhanced densities,
168 magnetic field strength and velocities. Particles from low to high energies showed the increase
169 of energy and enhanced fluxes. The shock produced compression caused the bow shock to move
170 inward at 16:49:36 UT, past the spacecraft as indicated by the decrease in the magnetic field
171 strength and, decrease in density and temperature and spectra expected for its entry into the solar
172 wind. THEMIS A observed the IP shock at 16:49:12 UT and in about 1 min and 34 s later its
173 magnetic field, density and temperature traces indicate that the bow shock moved inward past
174 THEMIS A.

175 Figures 4 (a, b) show GOES 13 and 15 observations of the magnetic field from 16:40 to
176 17:20 UT. Following the arrival of the transmitted IP shock at GOES 13 near local noon at
177 16:50:07 UT there was a sharp increase of magnetic field variations with amplitudes of ~ 70 nT
178 in the H component. The shock induced compression was so strong that at 17:02 UT GOES 13
179 briefly entered the sheath. The shock front was then detected at GOES 15 in the morning local
180 hours 33 sec later at 16:50:40 UT, where it caused a gradual increase of the magnetic field



181 amplitudes by ~ 20 nT followed by compressional pulsations that fall in the category of Pc5
182 pulsations.

183 The upper and middle panels of Figures 5 (a, b) present the Van Allen Probes A and B
184 magnetic field and electric observations from 16:40 to 17:20 UT. The arrival of the shock
185 characterized by a strong (~ 50 nT) increase in the total magnetic field strength and bipolar
186 variations in all three components of the electric field at $\sim 16:50:26$ UT at Probe B and 7 sec
187 later at Probe A. The initial electric field perturbations in the azimuthal component E_y observed
188 by Van Allen Probes A and B were directed downward with amplitudes of -9.4 and -8.2
189 mV/m, respectively, but ~ 4 minutes later the sense changed direction towards dusk (with
190 amplitudes of 5.3 and 5.8 mV/m). We interpret these variations as due to a compression of the
191 magnetosphere followed by a reflection [Samsonov et al., 2007]. The E_z and E_x components
192 show variations with amplitudes that are a factor of 1.5-2 smaller than those of the E_y
193 component. The bipolar electric field waveforms are followed by geomagnetic pulsations with
194 periods of ~ 330 s that damp within ~ 30 min.

195 Figures 6 (a, b) present Van Allen Probes A and B observations of the azimuthal
196 component of the electric field and pitch angle distributions of electron fluxes for energies at
197 31.5, 53.8, 108.3, 183.4, 231.8, and 342 KeV as measured by MagEIS instrument. The particles
198 exhibit enhanced fluxes of electrons at all energies but most intense at pitch angles $\sim 90^\circ$,
199 immediately after the arrival of the IP shock. Kanekal et al. [2016] suggested that the shock-
200 injection mechanism can be effective for energizing particles over substantial range of pitch
201 angles. One of the interesting features in Figures 6 is that the intensity of electrons in the
202 energy range of 31.5-342 KeV exhibits a regular periodicity with periods corresponding to
203 the ULF electric field waves. The oscillations in electron fluxes are in quadrature with the E_y
204 component. This component is of special interest because some charged particles that drift
205 azimuthally as a consequence of the gradient and curvature drifts in the Earth magnetic field can
206 traverse this electric field acquiring significant amount of energy. The initial flux enhancement
207 is more pronounced by comparison with the following pulses. We interpret these observations as
208 evidence for prompt energization of electrons due to shock induced ULF electric fields with an
209 additional contribution for the initial acceleration from the compressional effect of the shock
210 [Zong et al., 2009]. It should be noted that electrons can be accelerated most significantly



211 through a process known as drift resonance [Southwood and Kivelson, 1981] when resonant
212 particles drift with the same velocity as the wave front. Claudepierre et al. [2013] showed Van
213 Allen Probes observations of the energy dependence of the amplitude and phase of the electron
214 flux modulations which were consequences of drift resonance between ~ 60 keV electrons and
215 fundamental poloidal Pc5 waves. Hao et al. [2014] presented Van Allen Probes observations of
216 electron injections caused by the IP shock and showed that the injected electrons with energies
217 between 150 KeV and 230 KeV were in drift resonance with the excited poloidal ULF waves.
218 Considering the process for energizing drift resonant electrons, the value for the **EXB** drift
219 velocities of the particles in the wavefields provides important information. We calculated the
220 radial (V_x) and azimuthal (V_y) drift velocities at Van Allen Probes A and B for the interval
221 from 16:40 to 17:20 UT and present them in the two bottom panels of Figures 5 (a, b). The V_x
222 and V_y components associated with the minimum peak of the E_y electric field are about -40
223 km/s and -15 km/s for Van Allen Probe B and -35 km/s and -6 km/s for Van Allen Probe A, i.
224 e., the initial direction of the plasma flow is tailward and downward consistent with expectation
225 for the spiral orientation of the IP shock.

226 Knowing the distances between the satellites and the lag times for the propagation of shock
227 induced disturbances we calculated the shock propagation velocities. Table 1 summarizes the
228 onset times of the shock driven encounters at different spacecraft. In the solar wind Cluster 2
229 observed the shock earlier than Cluster 1, respectively, that is the shock moved downward.
230 The shock perturbations occurred almost simultaneously in the magnetosheath at Themis A and
231 D ($\Delta t < 12$ s) so we suppose that it hit the magnetopause somewhere between the two
232 spacecraft. The shock induced impulse propagated both dawnward and duskward (thick arrows
233 in Figure 2) from the point of origin on the magnetopause (depicted as an oval in Figure 2) that is
234 consistent with spiral orientation of the IP shock. In the outer magnetosphere the propagation
235 velocity for the disturbance was about 1348 km/s between Goes 13 and 15 but only about
236 390 km/s between Van Allen Probes B and A. We believe that the shock induced pulse
237 propagated with the velocity of fast mode waves. The local fast mode speed can be evaluated
238 from Van Allen Probe measurements of the magnetic field and density. At the time of the shock
239 encounter Van Allen Probes A and B were in the high-density plasmasphere at $L = 5.5$ and $L =$
240 5.1 , respectively. For a measured local magnetic field of 255 nT for Probe A and 220 nT for



241 Probe B and density of $\sim 200 \text{ cm}^{-3}$ derived from the potential of both spacecraft, the fast-mode
242 speeds will be $\sim 395 \text{ km/s}$ and 337 km/s , respectively, which are consistent with our estimates
243 of the propagation velocity derived from the time difference of shock arrivals at the spacecraft.
244 The decrease of the fast mode wave speed in the plasmasphere relative to that in the outer
245 magnetosphere agrees well with earlier studies [e.g., Wilken, 1982; Foster et al., 2016].

246

247 **Statistical study of shock-initiated signatures of the electric field**

248 In view of the importance of the electric field energizing particles we performed a statistical
249 study of E_y variations of the electric field and associated plasma drift V_x and V_y velocities
250 during the passage of interplanetary shocks. The list of IP shocks used in this study was obtained
251 from Heliospheric Shock Database maintained and generated by the University of Helsinki
252 [<http://ipshocks.fi>]. They identify shocks by visual inspection and an automated shock detection
253 algorithm. To be included in the database a shock should satisfy the following upstream to
254 downstream jump conditions: $B_{\text{down}}/B_{\text{up}} > 1.2$, $N_{\text{down}}/N_{\text{up}} > 1.2$, $T_{\text{down}}/T_{\text{up}} > 1/1.2$, for FF
255 $V_{\text{up}} - V_{\text{down}} > 20 \text{ km/s}$. The normal vector of the shock (n) was calculated from the magnetic
256 field data and velocities using the mixed mode method [Abraham-Shrauner and Yun, 1976].
257 When there is data gap in the velocity components the normal was calculated using magnetic
258 field coplanarity [Colburn and Sonett, 1966]. We identified more than 80 events observed by
259 Vann Allen Probes A and B associated with FF IP shocks for the period from 2013 to 2015.

260 The passage of a shock causes both electric and magnetic field perturbations and their
261 amplitudes to increase with the intensity of IP shocks. The initial peak to peak amplitudes of
262 the shock induced electric field variations ranged mostly from 0.8 mV/m to 6 mV/m and
263 lasted from 1.5 to 6 minutes. We classified their signatures into four different groups according
264 to the initial E_y electric field response to IP shocks. Figure 7 presents examples of observed E_y
265 variation, including a negative pulse, a negative-positive waveform, a positive pulse and
266 pulsations (upper panels) and the corresponding magnetic field response (bottom panels).
267 Figure 8 shows the GSM locations where event in each of these four groups were observed in
268 the X-Y plane. It provides evidence that they are local time dependent. The direction of the
269 initial E_y impulse is predominantly from the dusk-to-dawn direction in the dayside



270 magnetosphere, but in the dawn to dusk direction in the nightside magnetosphere within an L-
271 shell range of 3-5.

272 We used the formula $\mathbf{V} = \mathbf{E} \times \mathbf{B} / B^2$ to analyze the V_x and V_y flow velocities for the 30
273 events under the study for which the spin component E_x could be obtained from the $\mathbf{E} \cdot \mathbf{B} =$
274 0 assumption. Figure 9 presents the magnitude and direction of the plasma drift velocities V_x
275 observed by Probes A and B in response to interplanetary shocks (red- sunward and blue –
276 tailward directions). The direction of the V_x component of plasma flow is antisunward at all
277 local times except the nightside magnetosphere, where flows are sunward near the sun-Earth line
278 but antisunward towards dawn and dusk. Numbers show that the magnitudes of the flow
279 velocities V_x are a factor of 5 to 10 times stronger near noon (could reach 40 km/s) as this
280 region is fully exposed to compression that are shielded on the nightside.

281 Our results are consistent with the results of global 3D MHD code simulation for the
282 geosynchronous magnetic field response in the nightside magnetosphere to IP shocks by Wang
283 et al., [2010] presented in Figure 10. The figure shows contours of $\Delta |B_z|$ and velocity
284 vectors in the equatorial plane (blue regions - B_z negative, red regions - B_z positive). Their
285 model revealed that when a IP shock sweeps over the magnetosphere there are mainly two
286 regions in the nightside magnetosphere, a positive response region in B_z caused by the
287 compressive effect of the shock and a negative response region (blue) which is associated with
288 the temporary enhancement of earthward convection. They believe that the displacement of the
289 nightside magnetopause caused by the IP shock launches a flow in the magnetosphere near the
290 magnetopause that has a significant y-component, and converges toward the X axis. In the
291 vicinity of the Sun-Earth line at $\sim -5, -6 R_E$ the flow diverges, producing both an earthward
292 flow (consistent with the sunward direction of plasma flow in the nightside magnetosphere
293 presented in Figure 9) and a tailward flows.

294 As the direction of the shock normal should determine the direction of propagation of
295 transient perturbations and expected flow direction in the magnetosphere initiated by an IP shock
296 we categorize the events into two groups for spiral and orthospiral orientation of the shock
297 normal. Figure 11 presents the magnitude and direction of the plasma drift velocities V_y
298 observed by Van Allen Probes A and B in response to IP shocks (red- sunward V_x and blue –
299 tailward V_x directions) for spiral and orthospiral orientations of IP shocks. We excluded several



300 events from the list of shocks that lacked well defined shock normal. As anticipated, the
301 shock orientation controls the sense of dawn/dusk flows in magnetosphere. The observed
302 directions of azimuthal velocity V_y predominately agree with those expected for the given shock
303 normal orientation: dawnward for shocks that sweeps dawnward across the magnetosphere,
304 diskward for shocks that sweep duskward.

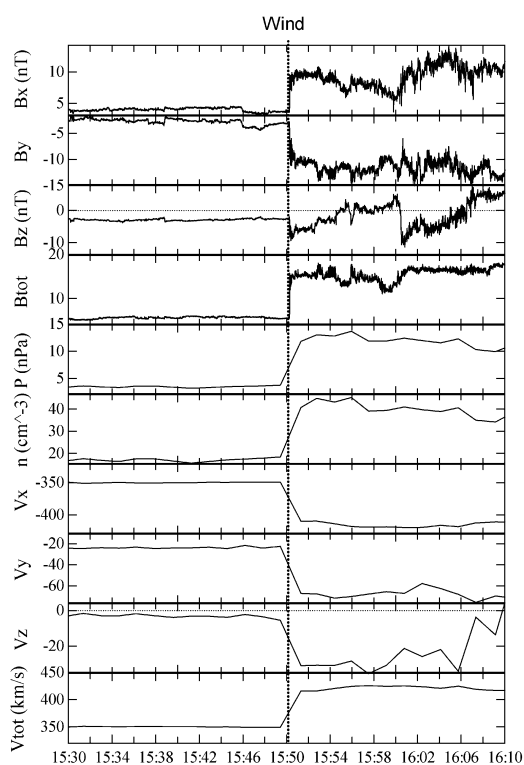
305 **Conclusions**

306 We studied multipoint observations of the electric, magnetic fields, plasma and particles in
307 response to an IP shock on February 27, 2014. We found that the initial encounter of the IP
308 shock with the magnetopause occurred on the early postnoon magnetosphere and the shock
309 induced impulse propagated as fast mode wave both dawnward and duskward from the point of
310 origin, that is consistent with spiral orientation of the IP shock. In the outer magnetosphere the
311 propagation velocity of disturbances was about 1348 km/s between Goes 13 and 15 in the
312 outer magnetosphere, but only about 390 km/s between Van Allen Probes B and A in the inner
313 magnetosphere. The multipoint measurements give evidence that the dayside equatorial
314 magnetosphere exhibited a dusk-dawn oscillatory electrical field with peak to peak amplitudes
315 of ~ 15 mV/m for a period of 30 min. The intensity of electrons in the energy range of 31.5 -
316 342 KeV shows a regular periodicity with periods corresponding to the shock induced ULF
317 electric field waves. The initial plasma flow velocity in the magnetosphere was directed
318 tailward and dawnward.

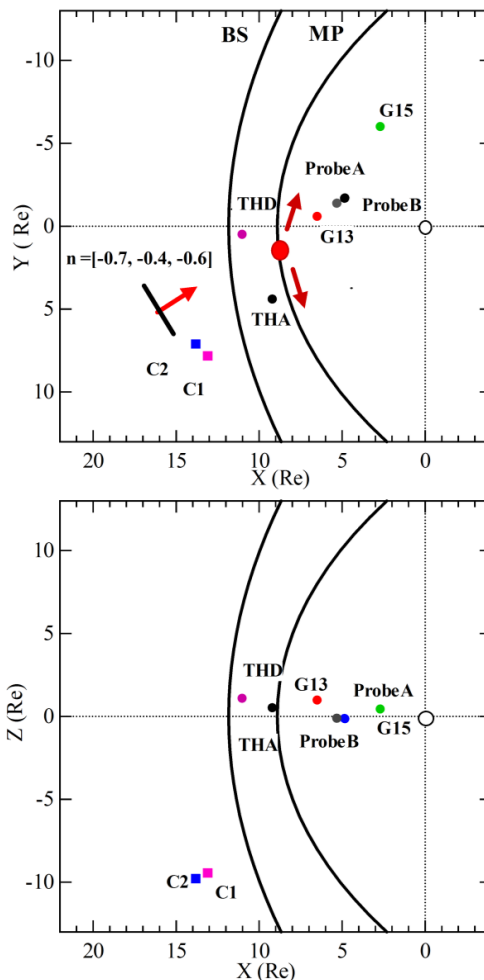
319 Then we performed a statistical study of E_y variations of the electric field and associated
320 plasma drift V_x and V_y flow velocities for 30 events during the passage of interplanetary shocks.
321 The initial peak to peak amplitudes of the transient electric field variations ranged mostly
322 from 0.8 mV/m to 6 mV/m and lasted from 1.5 to 6 minutes. As expected, flow velocity is
323 greatest near the local noon. We classified the shock-induced electric field signatures into four
324 different groups according to the initial E_y electric field response and provided evidence that
325 they are local time dependent. The direction of the V_x component of plasma flow is tailward at
326 all local times except the nightside magnetosphere, where flows are sunward near the Sun-Earth
327 line but antisunward towards dawn and dusk. The observed directions of azimuthal velocity V_y
328 predominately agree with those expected for the given spiral or orthospiral shock normal



329 orientation. Our results are consistent with the results of global 3D MHD code simulation of the
330 geosynchronous nightside magnetic field response to IP shock by Wang et al. [2010].
331
332
333

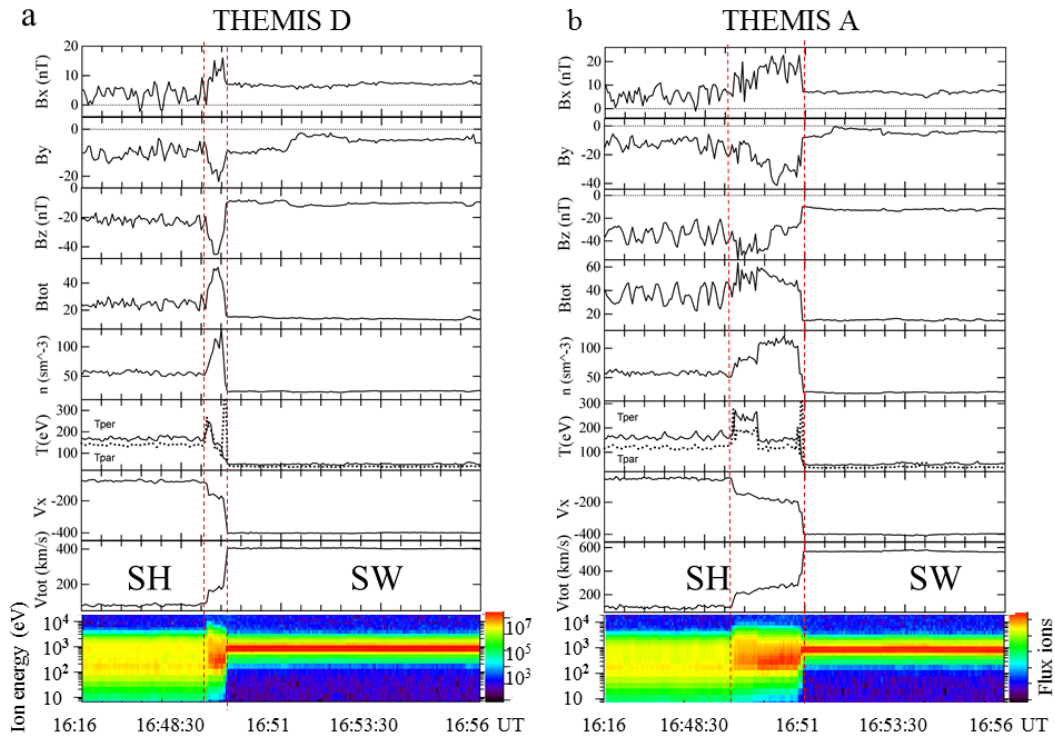


334
335 Figure 1. Wind observations of magnetic field and plasma in GSM coordinates from 15:30 UT
336 to 16:10 UT on February 27, 2014. Dashed line shows the time of arrival of an interplanetary
337 shock.



338

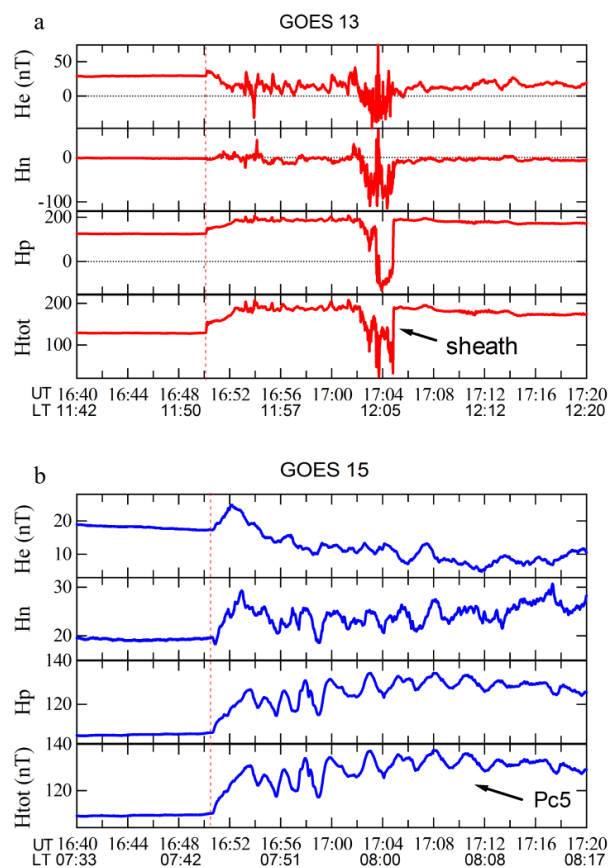
339 Figure 2. GSM locations of Cluster 1 and 2, THEMIS A, D, Van Allen Probes A and B and
 340 GOES 13 and 15 in the X-Y and Z-Y planes at ~1650 UT on February 27, 2014. The meaning
 341 of the solid oval and thick arrows will be discussed in the text later.



342
343

344 Figures 3 (a, b). THEMIS A (a) and THEMIS D (b) observations of magnetic field in GSM
345 coordinates plasma and energy spectra of ion fluxes from 16:16 UT to 16:56 UT on February
346 27, 2014.

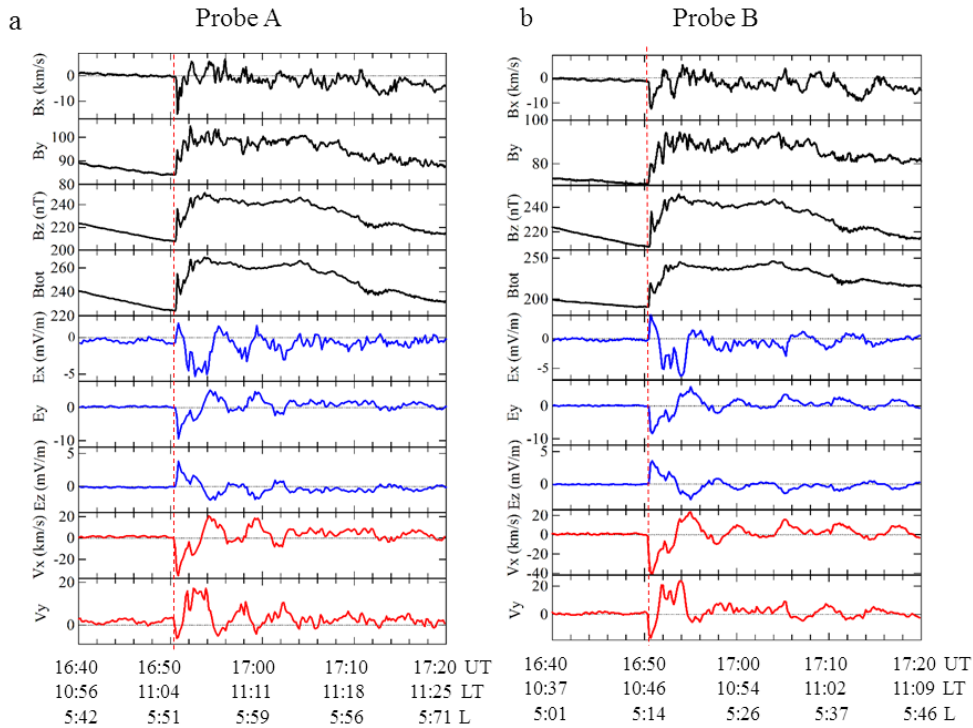
347



348

349 Figures 4 (a, b). GOES 13 (a) and GOES 15 (b) magnetic fields observations in PEN coordinate
350 from 16:40 UT to 17:20 UT on February 27, 2014. Hp is perpendicular to the satellite's orbital
351 plane, He pointing earthward parallel to the satellite-Earth center line, and Hn is perpendicular to
352 both Hp and He and pointing eastward.

353

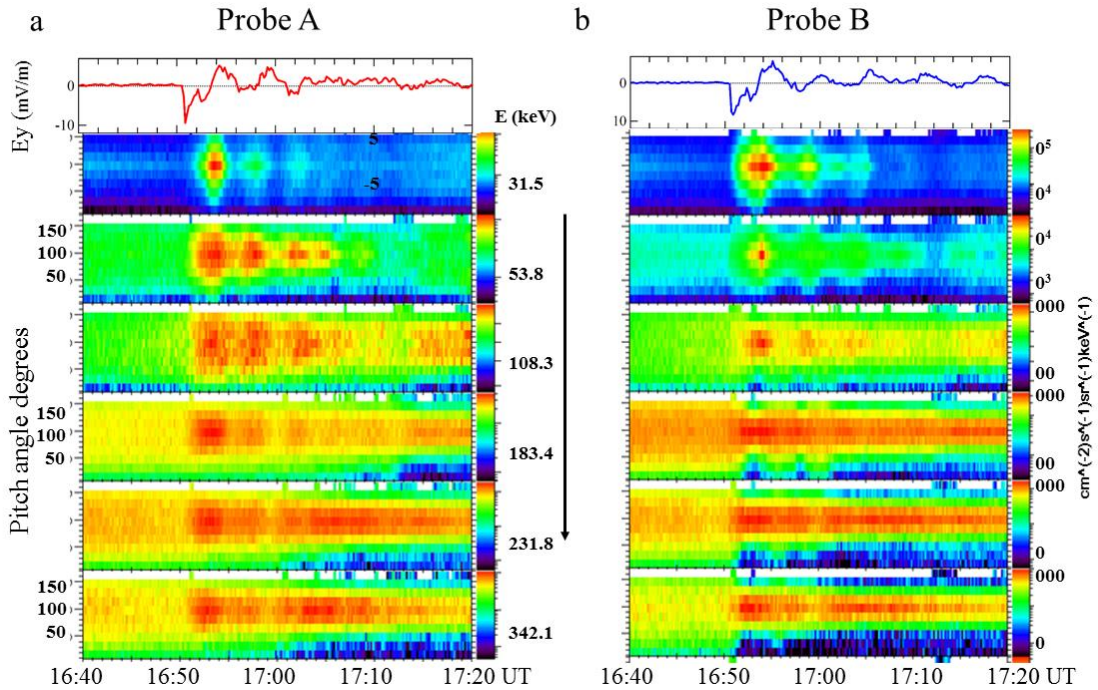


354

355 Figures 5 (a, b). Van Allen Probes A (a) and B (b) magnetic and spin-fit electric field
 356 observations and the V_x and V_y plasma flow velocities in GSE coordinates from 16:40 UT to
 357 17:20 UT on February 27, 2014.

358

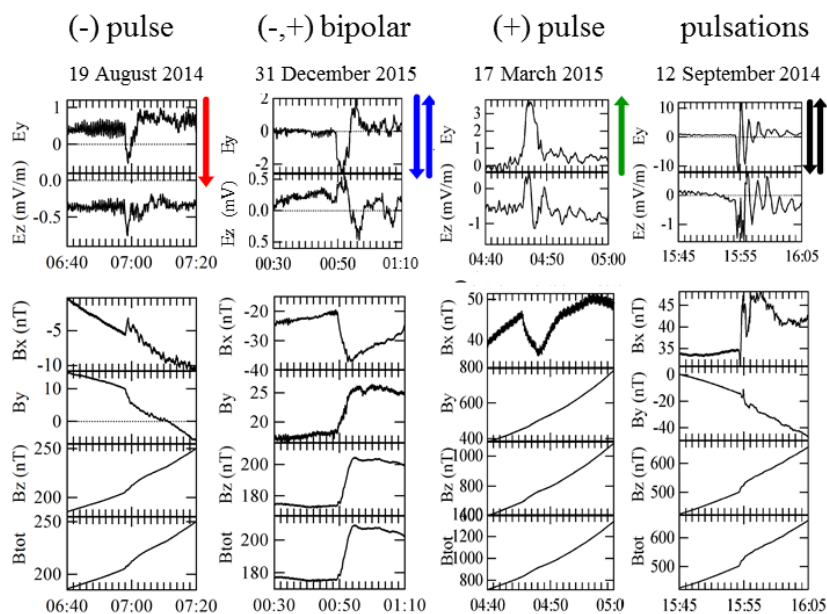
359



360

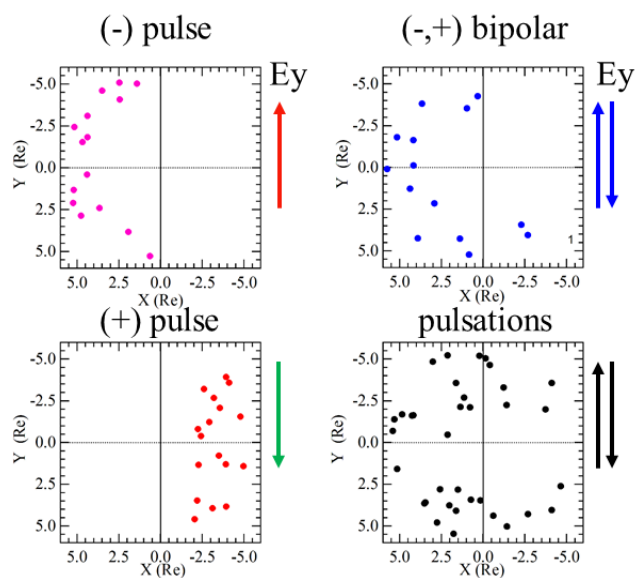
361 Figures 6 (a, b). Van Allen Probes A (a) and B (b) azimuthal component of the electric field
362 and pitch angle distributions of electron fluxes in the range of energies from 31.5 to 342 KeV,
363 measured by MagEIS instrument from 16:40 UT to 17:20 UT on February 27, 2014. The log
364 fluxes are color coded according to the color bar shown in the right panel.

365



366

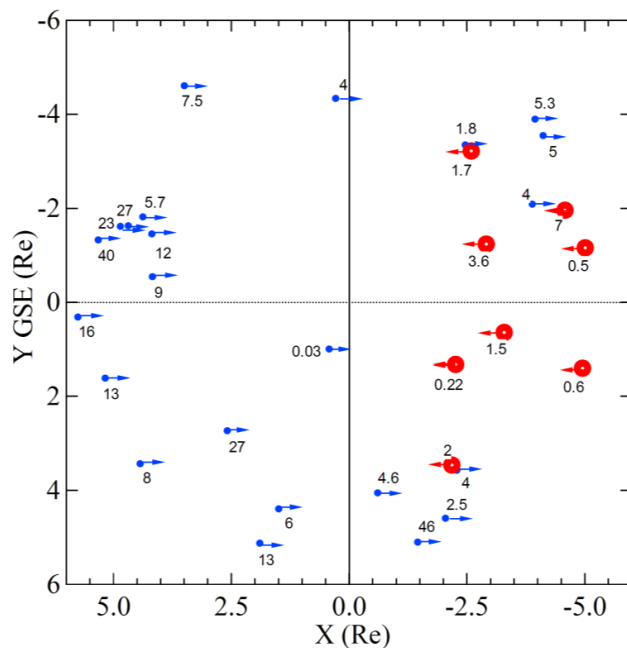
367 Figure 7. Examples of observed E_y initial variation, including a negative pulse, a negative-
 368 positive waveform, a positive pulse and pulsations (upper panels) and the corresponding
 369 magnetic field response (bottom panels).



370

371 Figure 8. GSM locations where event in each of the four groups were observed in the X-Y
372 plane.

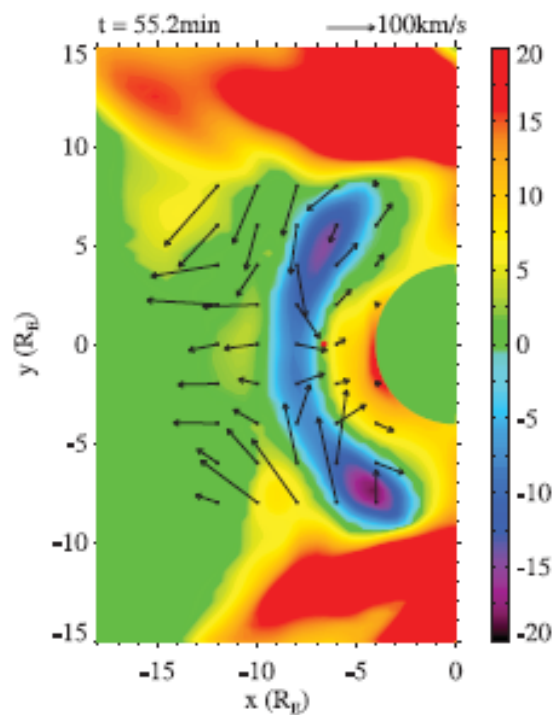
373



374

375 Figure 9. The magnitude and direction of the plasma drift velocities V_x observed by Van
376 Allen Probes A and B in response to interplanetary shocks (red - sunward and blue – tailward
377 directions). Numbers show their magnitudes.

378



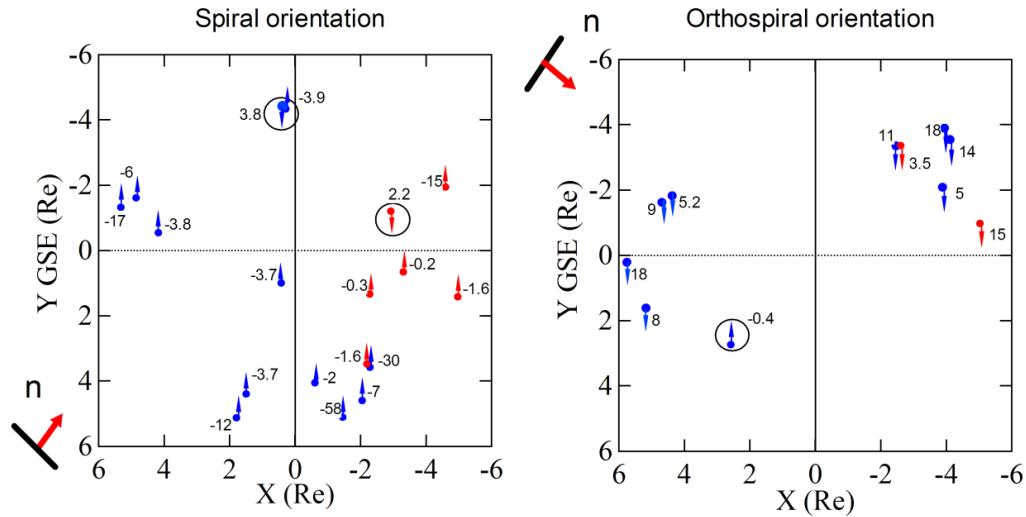
379

380 Figure 10. Results of nightside geosynchronous magnetic field response from the global MHD
381 code simulation of IP shock [Wang et al., 2010]. The arrows represent velocity vectors on the
382 equatorial plane.

383

384

385



386
 387 Figure 11. The magnitude and direction of V_y plasma drift velocities observed by Van Allen
 388 Probes A and B in response to interplanetary shocks for spiral and orthospiral orientations (red -
 389 sunward and blue – tailward V_x directions).

390 **Table 1. Times of encounter of the IP shock with the spacecraft and their locations in GSM**
 391 **coordinates**

392

S/C	Time	Position	GSM [X, Y, Z] Re	
Wind	15:50:12	220.90	93.92	31.49
Cluster 1	16:48:46	13.10	7.82	-9.44
Cluster 2	16:48:44	13.83	7.10	-9.78
THEMIS D	16:49:01	11.03	0.48	1.10
THEMIS A	16:49:12	9.22	4.39	0.53
Probe A	16:50:33	4.86	-1.69	0.12
Probe B	16:50:26	5.33	-1.39	-0.10
GOES 13	16:50:07	6.51	-0.60	0.99
GOES 15	16:50:40	2.71	-6.02	0.45

393



394

395 **Acknowledgements.** The Van Allen Probes mission is supported by NASA. NASA GSFC's
396 CDAWEB provided Wind and GOES observations, while SSCWEB provided Van Allen Probes
397 EPHEMERIS. The work by the EFW team was conducted under JHU/APL contract 922613
398 (RBSP-EFW). The work by G. Korotova at the University of Maryland was supported by grants
399 from NASA NNX15AW86G S01 and NSF AGS-1207445.

400

401 **References**

402

403 Abraham-Shrauner and Yun (1976), Interplanetary shocks seen by Ames Plasma Probe on
404 Pioneer 6 and 7, *J. Geophys. Res.*, 81, 2097-2102, DOI: 10.1029/JA081i013p02097.

405 Araki, T. (1994), A physical model of the geomagnetic sudden commencement, *AGU Geophys.*
406 *Monogr.*, 81, 183–200.

407 Auster, H. U., et al. (2008), The THEMIS Fluxgate Magnetometer, *Space Sci. Rev.*, 141, 235–
408 264, DOI:10.1007/s11214-008-9365-9.

409 Blake, J B, Carranza P A, Claudepierre S G, Clemmons J H, Crain W R, et al. (2013),The
410 Magnetic Electron Ion Spectrometer (MagEIS) Instruments Aboard the Radiation Belt
411 Storm Probes (RBSP) Spacecraft, *Space Sci. Rev.*,179, 383-421, DOI: 10.1007/s11214-
412 013-9991-8.

413 Bonnell, J. W., F. S. Mozer, G. T. Delory, A. J. Hull, R. E. Ergun, C. M. Cully, V. Angelopoulos, and P. R.
414 Harvey (2008), The electric field instrument (EFI) for THEMIS, *Space Sci. Rev.*, 141, 303–341,
415 DOI:10.1007/s11214-008-9469-2.

416 Claudepierre, S. G., et al., (2013), Van Allen Probes observation of localized drift resonance
417 between poloidal mode ultra-low frequency waves and 60 keV electrons. *Geophys. Res.*
418 *Lett.* 40, 4491–4497, DOI:10.1002/grl.50901.

419 Colburn, D.C., and C. P. Sonett, (1966), Discontinuities in the solar wind, *Space Science*
420 *Reviews*, 5(4):439–506.

421 Foster, J., J. Wygant, M. Hudson, A. Boyd, D. Baker, P. Erickson, H.E. Spence, (2015), Shock-
422 induced prompt relativistic electron acceleration in the inner magnetosphere. *J. Geophys.*
423 *Res.* 120(3), 1661–1674, DOI:10.1002/2014JA020642.



- 424 Glassmeier, K. H., C. Heppner (1992), Travelling magnetospheric twin-vortices: Another
425 case study, global characteristics and a model. *J. Geophys. Res.* 97, 3977-3992. DOI:
426 10.1029/91JA02464.
- 427 Guo, X. C., Y. Q. Hu, and C. Wang (2005), Earth's magnetosphere impinged by interplanetary shocks of
428 different orientations, *Chin. Phys. Lett.*, 22, 3221–3224.
- 429 Halford, A.J., S.L. McGregor, K.R. Murphy, R.M. Millan, M.K. Hudson, L.A. Woodger, C.A.
430 Cattel, A.W. Breneman, I.R. Mann, W.S. Kurth, G.B. Hospodarsky, M. Gkioulidou, J.F.
431 Fennell, (2015), BARREL observations of an ICME-Shock impact with the magnetosphere
432 and the resultant radiation belt electron loss. *J. Geophys. Res. Space Phys.*, *J. Geophys. Res.*,
433 120, 2557–2570, DOI:10.1002/2014JA020873.
- 434 Hao, Y., Q.-G. Zong, Y. Wang, X.-Z. Zhou, H. Zhang, S. Fu, Z. Y. Pu, H. E. Spence, J. B.
435 Blake, J. Bonnell, J. Wygant, and C. Kletzing, (2014), Interactions of energetic electrons
436 with ULF waves triggered by interplanetary shock: Van Allen Probes observations in
437 the magnetotail, *J. Geophys. Res.*, DOI: 10.1002/2014JA020023.
- 438 Kanekal, S. G., D. N. Baker, J. F. Fennell, A. Jones, Q. Schiller, I. G. Richardson, X. Li, D. L.
439 Turner, S. Califf, S. G. Claudepierre, L. B. Wilson III, A. Jaynes, J. B. Blake, G. Reeves, H.
440 E. Spence, C. A. Kletzing, and J. R. Wygant, (2016), Prompt Acceleration of
441 Magnetospheric Electrons to Ultra-Relativistic Energies by the 17 March 2015
442 Interplanetary Shock, *J. Geophys. Res.*, DOI:10.1002/2016JA022596.
- 443 Kim, K.-H., K. S. Park, T. Ogino, D.-H. Lee, S.-K. Sung, and Y.-S. Kwak (2009), Global MHD
444 simulation of the geomagnetic sudden commencement on 21 October 1999, *J. Geophys. Res.*,
445 114, A08212, DOI:10.1029/2009JA014109.
- 446 Kletzing, C. A., Kurth, W. S., Acuna, M., MacDowall, R. J, Torbert, R. B., Averkamp, T., Bodet,
447 D., Bounds, S. R., Chutter, M., Connerney, J., Crawford, D., Dolan, J. S., Dvorsky R.,
448 Hospodarsky, G. B., Howard, J., Jordanova, V., Johnson, R. A., Kirchner, D. L., Mokrzycki,
449 B., Needell, G., Odom, J., Mark, D., Pfaff Jr., Phillips, J. R. , Piker, C.W., Remington, S. L.,
450 Rowland, D., Santolik, O., Schnurr, R., Sheppard, D., Smith, C. W., Thorne, R. M., and
451 Tyler, J. J. (2013), The Electric and Magnetic Field Instrument Suite and Integrated Science
452 (EMFISIS) on RBSP, *Space Sci. Rev.*, 179, 127–181, DOI:10.1007/s11214-013-9993-6.



- 453 Knott, K., D. Fairfield, A. Korth, and D. T. Young (1982), Observations near the magnetopause
454 at the onset of the July 29, 1977, sudden storm commencement, *J. Geophys. Res.*, 87, A8,
455 5888–5894, DOI: 10.1029/JA087iA08p05888.
- 456 Li, X., I. Roth, M. Temerin, J.R. Wygant, M.K. Hudson, J.B. Blake (1993), Simulation of the
457 prompt energization and transport of radiation belt particles during the March 24, 1991 ssc.
458 *Geophys. Res. Lett.* 20, 2423–2426, DOI: 10.1029/93GL02701.
- 459 Mitchell, D.G., Lanzerotti, L.J., Kim, C.K., Stokes, M., Ho, G., Cooper, S., Ukhorskiy, A.,
460 Manweiler, J.W., Jaskulek, S., Haggerty, D.K., Brandt, P., Sitnov, M., Keika, K., Hayes,
461 J.R., Brown, L.E., Gurnee, R.S., Hutcheson, J.C., Nelson, K.S., Paschalidis, N., Rossano,
462 E., Kerem, S. (2013). Radiation Belt Storm Probes Ion Composition Experiment
463 (RBSPICE), *Space Sci Rev.*, 179, 263-308, DOI:10.1007/s11214-013-9965-x.
- 464 Mauk, B. H., Fox, N. J., Kanekal, S. G., Kessel, R. L., Sibeck, D. G., and Ukhorskiy, A (2012),
465 Science objectives and rationale for the radiation belt storm probes mission, *Space Sci. Rev.*,
466 179, 3–27, DOI:10.1007/s11214-012-9908-y.
- 467 McFadden, J. P., C. W. Carlson, D. Larson, M. Ludlam, R. Abiad, B. Elliott, P. Turin, M.
468 Marckwordt, and V. Angelopoulos (2008), The THEMIS ESA plasma instrument and in-
469 flight calibration, *Space Sci. Rev.*, 141, 277, DOI:10.1007/s11214-008-9440-2.
- 470 Nopper, R. W., Jr., W. J. Hughes, C. G. MacLennan, and R. L. McPherron (1982), Impulse-
471 excited pulsations during the July 29, 1977, event, *J. Geophys. Res.*, 87 (A8), 5911-5916,
472 DOI: 10.1029/JA087iA08p05911.
- 473 Ogilvie, K. W., et al. (1995), SWE, a comprehensive plasma instrument for the WIND spacecraft, *Space*
474 *Sci. Rev.*, 71, 55–77, DOI:10.1007/BF00751326.
- 475 Oliveira, D. M., and Joachim Raeder (2015), *J. Geophys. Res.*, Impact angle control of
476 interplanetary shock geoeffectiveness: A statistical study, 120, 6, 4313–4323, DOI:
477 10.1002/2015JA021147.
- 478 Samsonov, A. A., D. G. Sibeck, and J. Imber (2007), MHD simulation for the interaction of an
479 interplanetary shock with the Earth's magnetosphere, *J. Geophys. Res.*, 112, A12220, DOI:
480 10.1029/2007JA012627.
- 481 Schiller, O., S. G. Kanekal, L. K. Jian, X. Li, A. Jones, D. N. Baker, A. Jaynes, and H. E.
482 Spence (2016), Prompt injections of highly relativistic electrons induced by interplanetary



- 483 shocks: A statistical study of Van Allen Probes observations, *Research Letter*,
484 10.1002/2016GL071628.
- 485 Schmidt, R., A. Pedersen, (1988), Signatures of storm sudden commencements in the electric
486 field measured at geostationary orbit (GEOS-2), *Phys. Scr.*, 37, 3, 491–495.
- 487 Shinbori, A., T. Ono, M. Iizima, A. Kumamoto, and H. Oya (2003), Sudden commencements related
488 plasma waves observed by the Akebono satellite in the polar region and inside the plasmasphere
489 region, *J. Geophys. Res.*, 108, A12, 1457, DOI:10.1029/2003JA009964.
- 490 Shinbori, A., T. Ono, M. Iizima, and A. Kumamoto (2004), SC related electric and magnetic field
491 phenomena observed by the Akebono satellite inside the plasmasphere, *Earth Planets Space*, 56,
492 269–282.
- 493 Sibeck, D. G. (1990), A model for the transient magnetospheric response to sudden solar wind
494 dynamic pressure variations. *J. Geophys. Res.* 95, A4, 3755–3771,
495 DOI:10.1029/JA095iA04p03755.
- 496 Singer, H. J., L. Matheson, R. Grubb, A. Newman, and S. D. Bouwer (1996), Monitoring space weather
497 with the GOES magnetometers, *Proc. SPIE Int. Soc. Opt. Eng.*, 2812, 299–308.
- 498 Southwood, D. J., and M.G. Kivelson (1982), Charged particle behavior in low-frequency
499 geomagnetic pulsations: 2. Graphical approach. *J. Geophys. Res.* 87, 1707–1710, DOI:
500 10.1029/JA087iA03p01707.
- 501 Southwood, D. J., and M. G. Kivelson (1981), Charged particle behavior in low-frequency
502 geomagnetic pulsations: 1. Transverse waves, *J. Geophys. Res.*, 86, 5643–5655, DOI:
503 10.1029/JA086iA07p05643.
- 504 Southwood, D. J., and M. G. Kivelson (1990), The Magnetohydrodynamic Response of the
505 Magnetospheric Cavity to Changes in Solar Wind Pressure, *J. Geophys. Res.* 95, 2301–
506 2309, DOI: 10.1029/JA095iA03p02301.
- 507 Southwood, D. J., and M. Kivelson (1991), An approximate description of field-aligned currents in a
508 planetary magnetic field, *J. Geophys. Res.*, 96, 67-75, DOI:10.1029/90JA01806.
- 509 Spence, H. E., G. D. Reeves, D. N. Baker, J. B. Blake, M. Bolton, S. Bourdarie, A. H. Chan, S.
510 G. Claudepierre, J. H. Clemmons, J. P. Cravens, S. R. Elkington, J. F. Fennell, R. H. W.
511 Friedel, H. O. Funsten, J. Goldstein, J. C. Green, A. Guthrie, M. G. Henderson, R. B. Horne,
512 M. K. Hudson, J.-M. Jahn, V. K. Jordanova, S. G. Kanekal, B. W. Klatt, B. A. Larsen, X. Li,



- 513 E. A. MacDonald, I. R. Mann, J. Niehof, T. P. O'Brien, T. G. Onsager, D. Salvaggio, R. M.
514 Skoug, S. S. Smith, L. L. Suther, M. F. Thomsen, and R. M. Thorne, (2013), Science Goals
515 and Overview of the Energetic Particle, Composition, and Thermal Plasma (ECT) Suite on
516 NASA's Radiation Belt Storm Probes (RBSP) Mission, *Space Sci. Rev.*, DOI:
517 10.1007/s11214-013-0007-5.
- 518 Takahashi, N., Y. Kasaba, Y. Nishimura, A. Shinbori, T. Kikuchi, T. Hori, Y. Ebihara, and N.
519 Nishitani (2017), Propagation and evolution of electric fields associated with solar wind
520 pressure pulses based on spacecraft and ground-based observations,
521 DOI:10.1002/2017JA023990.
- 522 Tamao, T. (1964), The structure of three-dimensional hydromagnetic waves in a uniform cold
523 plasma, *J. Geomagn. Geoelectr.*, 48, 89–114, DOI <https://doi.org/10.5636/jgg.16.89>.
- 524 Wang, C., T. R. Sun, X. C. Guo, and J. D. Richardson (2010), Case study of nightside magnetospheric
525 magnetic field response to interplanetary shocks, *J. Geophys. Res.*, 115, A10247,
526 DOI:10.1029/2010JA015451.
- 527 Wilken, W., C.K. Goertz, D.N. Baker, P.R. Higbie, T.A. Fritz (1982), The SSC on July 29,
528 1977 and its propagation within the magnetosphere. *J. Geophys. Res.* 87, 5901–5910, DOI:
529 10.1029/JA087iA08p05901.
- 530 Wilken, W., D.N. Baker, P.R. Higbie, T.A. Fritz, W.P. Olson, K.A. Pfizter (1986),
531 Magnetospheric configuration and energetic particle effects associated with a SSC: A case
532 study of the CDAW event on March 22, 1979, *J. Geophys. Res.* 91, 1459–1473, DOI:
533 10.1029/JA091iA02p01459.
- 534 Wygant, J., F. Mozer, M. Temerin, J. Blake, N. Maynard, H. Singer, and M. Smiddy (1994), Large
535 amplitude electric field and magnetic field signatures in the inner magnetosphere during
536 injection of 15 MeV electron drift echoes, *Geophys. Res. Lett.*, 21, 1739–1742, DOI:
537 10.1029/94GL00375.
- 538 Wygant, J. R., Bonnell, J. W., Goetz, K., Ergun, R. E., Mozer, F. S., Bale, S. D., Ludlam, M.,
539 Turin, P., Harvey, P. R., Hochmann, R., Harps, K., Dalton, G., McCauley, J., Rachelson,
540 W., Gordon, D., Donakowski, B., Shultz, C., Smith, C., Diaz-Aguado, M., Fischer, J.,
541 Heavner, S., Berg, P., Malaspina, D. M., Bolton, M. K., Hudson, M., Strangeway, R. J.,
542 Baker, D. N., Li, X., Albert, J., Foster, J. C., Chaston, C. C., Mann, I., Donovan, E., Cully,
543 C. M., Cattell, C. A., Krasnoselskikh, V., Kersten, K., Breneman, A., and Tao, J. B. (2013),



544 The electric field and waves instruments on the radiation belt storm probes mission, Space
545 Sci. Rev., 179, 183–220, DOI:10.1007/s11214-013-0013-7.

546 Zong, Q.-G., X.-Z. Zhou, Y. F. Wang, X. Li, P. Song, D. N. Baker, T. A. Fritz, P. W. Daly, M. Dunlop,
547 and A. Pedersen (2009), Energetic electron response to ULF waves induced by interplanetary
548 shocks in the outer radiation belt, J. Geophys. Res., 114, A10204,
549 DOI:10.1029/2009JA014393.